Proceedings of ASME TURBO EXPO 2004
Power for Land, Sea, and Air
June 14-17, 2004, Vienna, Austria

GT2004-53256

AXIAL TURBINE TIP DESENSITIZATION BY INJECTION FROM A TIP TRENCH

PART 1: EFFECT OF INJECTION MASS FLOW RATE

Nikhil M. Rao[1], Cengiz Camci[2]

Turbomachinery Heat Transfer Laboratory
Department of Aerospace Engineering
The Pennsylvania State University

223 Hammond Building, University Park, PA 16802

ABSTRACT

An experimental study of a turbine tip desensitization method based on tip coolant injection was conducted in a large-scale rotating turbine rig. One of twenty-nine rotor blades was modified and instrumented to have a tip trench with discrete injection holes directed towards the pressure side. Time accurate absolute total pressure was measured 0.3 chord lengths downstream of the rotor exit plane using a fast response dynamic pressure sensor in a phase-locked manner. The test cases presented include results for tip gap heights of 1.40% and 0.72% of the blade height, and coolant injection rates of 0.41%, 0.52%, 0.63%, and 0.72% core mass flow rate. At a gap height of 1.40% the leakage vortex is large, occupying about 15% blade span. A reduction in gap height causes the leakage vortex to reduce in size and move towards the blade suction side. The minimum total pressure measured, for the reduced gap, in the leakage vortex is about 4% greater. Coolant injection from the tip trench is successful in filling in the total pressure defect originally resulting from the leakage vortex without injection. At the higher tip injection rates the leakage vortex is also seen to have moved towards the blade tip. The high momentum associated with the tip jets affects the total pressure distributions in the neighboring passages.

INTRODUCTION

An important source of efficiency loss in turbine rotors is the gap that exists between the rotating blades and the stationary casing. This gap, also termed as the tip clearance, allows the working fluid to flow from blade pressure to suction side mainly due to the pressure difference. The leakage flow does not follow the primary, work-generating path thereby directly reducing the power generated and the stage efficiency. In addition, the leakage jet approaches the suction side of the passage at an incidence to the primary flow direction giving rise to losses due to mixing, Bindon [1]. The tip clearance flow rolls up into a vortex, blocking the passage flow. According to Booth et al. [2] the losses due to tip clearance can be as high as a third of the stage losses. Tip clearance flows also have a severe thermal effect on the tip platform, Bindon [3]. The high velocity associated with the leakage flow leads to higher heat transfer coefficients on the tip platform, particularly in the pressure side corner. The amount of heat transferred to the tip platform is also higher since the leakage flow originates from fluid that does not generate significant work. These problems are particularly severe in HP stages where the use of shrouded blades is uncommon due to mechanical and cooling constraints. High pressure stages are typically characterized by low aspect ratios, with the tip gap forming a larger percent of the blade height compared to other stages. An extensive review of the aero-thermal aspects of the tip gap problem can be found in Bunker [4].

Reducing the detrimental effects of tip leakage flows is generally referred to as tip desensitization. One of the most common methods is that of employing full squealer tips. The flow passing over the pressure side of the blade encounters a sudden expansion as it enters the squealer cavity, thereby generating significant total pressure loss in this re-circulatory flow zone. A numerical investigation by Yang et al. [5] shows that the leakage flow rate over a squealer tip is less than that of a flat tip with the same clearance gap. However, this difference is minimal at higher gap heights. Other concepts that have been reported in available literature include the use of partial squealers, winglets that are also termed as "tip platform extensions", tip chamfering, and camber line sealing strips. Dey et al. [6, 7, 8] experimentally evaluated the effects of partial squealers and tip platform extensions in a large scale rotating rig turbine rig at the Pennsylvania State University.

1 *Research Assistant, Pennsylvania State University, nmr2@psu.edu*
2 *Professor of Aerospace Engineering, Pennsylvania State University, cxc11@psu.edu*

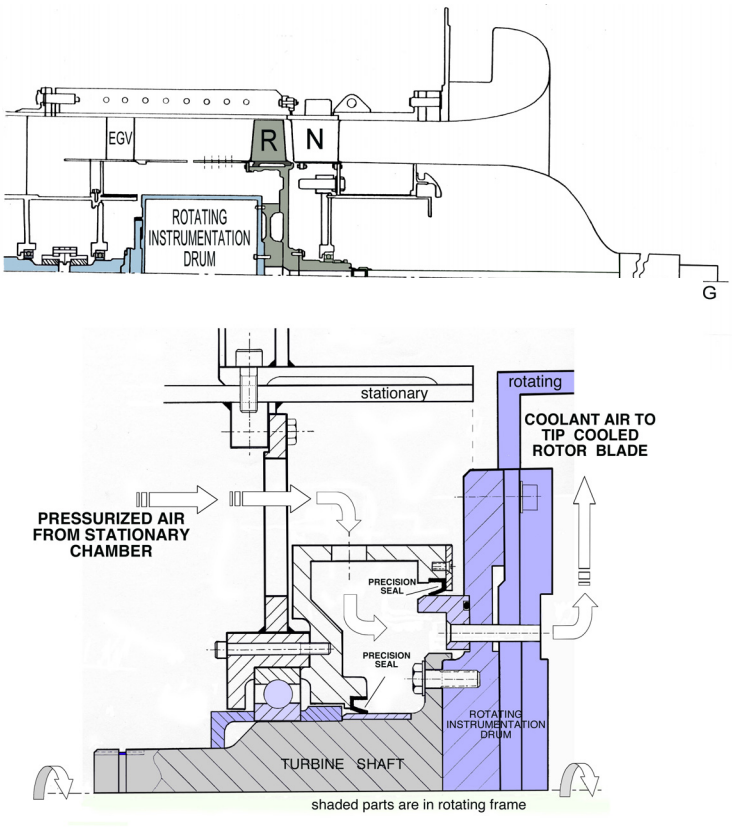

Figure 1 Axial Flow Turbine Research Facility (AFTRF) and coolant air transfer system for blade tip injection

Pressure-side extensions were found to be more effective than the suction-side extensions in weakening the tip vortex forming near the suction-side corner of the blade tip. Booth et al. [2] came to similar conclusions in using blade tip extensions or winglets. According to Dey et al. [8], partial squealer rims applied near the suction-side of turbine blade tips were more effective than pressure-side squealers in recovering the total pressure in the core of the tip vortex. An important conclusion in [6] similar to that of Yang et al. [5], was that squealer performance is best at small tip clearances. Dey [9] also reported a preliminary investigation of tip desensitization by coolant injection from a tip trench in a large scale rotating rig. A coolant mass flow of 0.3% core flow was investigated and was found to have no measurable effect on the tip leakage flow.

Tallman et al. [10] computationally investigated a number of turbine tip geometry modifications. The modifications consisted of chamfering the tip gap region from pressure-side to suction-side, thus creating a diffusing section in the leakage flow path. Chamfering near the leading edge led to increased leakage vortex activity and losses, while chamfering near the trailing edge reduced the vortex size. This was attributed to turning of gap flow towards the camber-line. Chamfering the entire length of the gap caused higher losses due to larger vortex. The effects of radiused pressure-side edge and camber-line strip were numerically investigated by Ameri [11]. It was found that the sharp edge tip was more successful, than the radiused edge, in reducing the tip leakage. The mean camber-line strip reduced the leakage mass flow when implemented with a radiused edge. However, the authors note that the reduction in total pressure loss was not proportionate. An implementation of chord-wise sealing strips on a turbine tip was also presented by Bunker et al. [12].

Modern HP turbine stages typically exhaust coolant, via radial holes through the tip platform. This was numerically investigated by Chen et al. [13]. They concluded that a secondary jet injected normal to leakage flow was successful in reducing the tip leakage mass flow rate. The current investigation develops on the work of Dey [9]. Coolant air is injected from discrete holes in a tip trench, with the holes being angled towards (at 45^0) the blade pressure side. The high momentum jets are diffused in the trench and they are expected to block and deflect the tip leakage flow. Discrete hole injection is expected to reduce the leakage mass flow and eventually limit mixing losses due to leakage vortex. At lower injection rates it is expected that the spreading of the jets will either locally form a film, causing the leakage flow to pass over it or the leakage flow will drag the low momentum coolant fluid further into the gap. Thus, there are potential thermal benefits, not investigated in this research. The effect of mass injection is observed by the local changes in the absolute total pressure field at the rotor exit. Four different injection flow rates are presented.

FACILITY DESCRIPTION

Turbine Research Facility: The facility used for the current research is the Axial Flow Turbine Research Facility (AFTRF) as shown in Fig. 1. A detailed description of the design of this rig is available in Lakshminarayana et al. [14]. Briefly, the AFTRF is a continuously operating, cold turbine rig designed to produce 60.6 kW. It consists of a single stage axial turbine followed by a 4-stage axial fan section used as a suction blower. The turbine power output is absorbed by an eddy current brake. Power is transferred from the turbine shaft to the brake shaft by a belt & pulley system. The brake can control turbine speed to within ± 1 rpm. . The important turbine design data are listed in Tables (1) and (2) respectively.

Table 1 AFTRF Facility Performance Data

Inlet Total Temperature;T_{o1} (K)	289
Inlet Total Pressure;P_{o1} (kPa)	101.36
Mass Flow Rate;Q (kg/sec)	11.05
Rotational Speed; N (rpm)	1300
Total Pressure Ratio; P_{o1}/P_{o3}	1.0778
Total Temperature Ratio; T_{o3}/T_{o1}	0.981
Pressure Drop; P_{o1}-P_{o3} (mm Hg)	56.04
Power; P (kW)	60.6

Air Transfer System: The lower sketch in Fig. 1 describes the air transfer system used for bringing the tip coolant air from the stationary frame to blade tip section in the rotor frame of reference. A custom designed rotating air chamber is located near the downstream bearing of the turbine rotor assembly. The two precision seal systems provide minimized leakage between the rotating and stationary surfaces of the air transfer system.

Table 2 AFTRF Stage Blade & Vane Data

Rotor hub-tip ratio	0.7269
Blade Tip Radius; R_{tip} (m)	0.4582
Blade Height; h_b (m)	0.1229
Rotor Blade:	
Relative Mach Number	0.24
Number of Blades	29
Chord; (m)	0.1287
Axial Tip Chord; (m)	0.085
Spacing; (m)	0.1028
Turning Angle; Tip / Hub	95.42^o / 125.69^o
Tip Clearance; (mm)	0.9
Reynolds Number ($\div 10^5$) inlet / exit	(2.5~4.5) / (5~7)
Nozzle Vane:	
Number of Vanes	23
Chord; (m)	0.1768
Spacing; (m)	0.1308
Turning Angle;	70^o
Reynolds Number ($\div 10^5$) inlet / exit	(3~4) / (9~10)

The two stationary seals work against plasma coated surfaces on the turbine shaft and rotating drum of the AFTRF. Although the leaks at the two seal locations are minimized, the coolant air mass flow rate is also measured by an individual orifice in the rotating frame after the air transfer system (just before the blade entry).

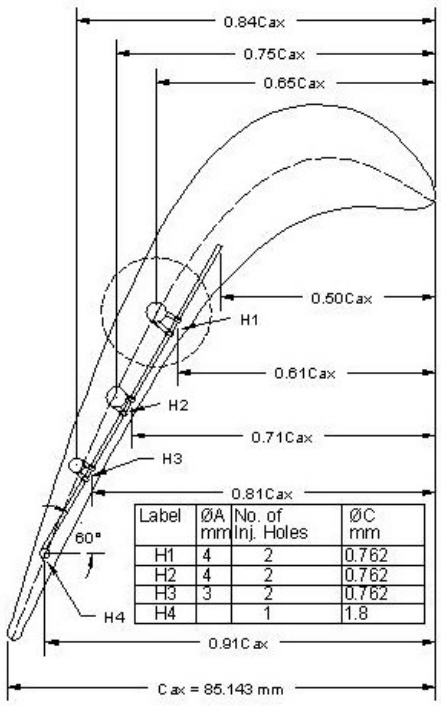

Figure 2-a Geometry of Tip Trench

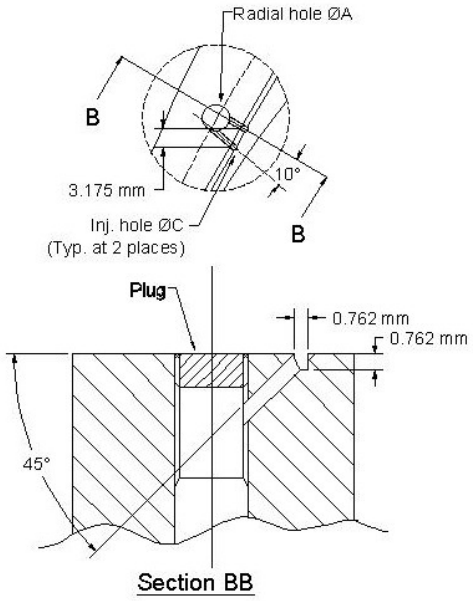

Figure 2-b Geometry of Injection Holes

Tip Cooled Rotor Blades: The rotor consists of 29 blades, with a design clearance of t/h=0.73%. Five adjacent blades were previously modified, with the tip clearance for each of these blades increased to a nominal value of 1.40% of blade height. Additionally, a tip trench was machined into each of these blades and injection holes at four locations 61%, 71%, 81%, and 91% blade axial chord were drilled into the tip trench. Geometrical details of one of these five blades with a tip trench and injection holes are shown in Figures 2-a and 2-b. A common plenum at the blade root supplies the injection air into four individual radial plenums feeding into hole locations H1, H2, H3 and H4 as defined in Fig. 2-a. Tip cooling plenums in the radial direction are also shown in Fig. 2-c. For the results reported in this paper, only one of the modified blades is used for tip injection purposes. This blade is referred to as the "test blade". Thermoplastic precision shims are attached to the tip platforms of the other four modified blades. It must be noted that for the remaining 28 blades, the minimum t/h = 0.71%, the maximum t/h = 0.92%, and the mean t/h = 0.83%. On the test blade, at 91% chord, the injection hole is a single radial hole (H4) that opens directly into the blade plenum. The diameter of H4 is 1.8 mm. At each of the other three locations two discrete holes of diameter 0.76 mm, inclined towards the blade pressure-side at 45° to the tip platform are drilled. Each set of 0.76 mm holes opens into a separate sub-plenum. The common blade plenum is connected to the air transfer system via high strength nylon tubing. Nylon tubing from each modified blade is fitted onto barbed fittings on the disk. The air supply to the air transfer system is maintained by a pressure regulator on an external tank.

Instrumentation: Instruments used for monitoring the turbine performance parameters consist of thermocouples, wall static holes and Pitot probes. Total temperature probes with K-type thermocouples installed in the bell-mouth inlet and downstream of the rotor measure the total temperatures at these stations.

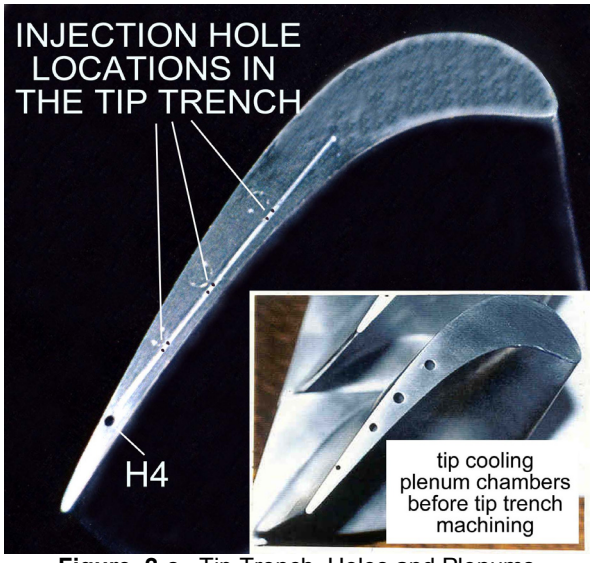

Figure 2-c Tip Trench, Holes and Plenums

The thermocouples are connected to Omega 650 and DP116 temperature readers. The inlet and exit total pressures at the same locations are also measured. The pressure ports are connected to Data Instruments model XCX pressure transducers. The transducers are calibrated against a Dwyer Instruments Inc., manometer. A BEI optical shaft encoder, Model H25, with a one per rev. pulse and a 6000 per rev. pulse is mounted on the turbine shaft. The 6000 per rev. pulse is used to measure the turbine speed via a frequency counter on a HP 5326B Timer-Counter-DVM. The measurement bins in the ensemble averaging process are also defined using the 6000 per rev. signal of the encoder. Injection mass flow rate is measured by a calibrated orifice plate installed on the supply line in the rotating frame of reference. The orifice plate is calibrated against a Dwyer Instruments Inc., flow meter in terms of standard volume flow rate. The pressure taps on the orifice plate are connected to a PSI Systems ESP-48 pressure transducer mounted in the rotating frame. The transducer has a range of ±1psi and has a maximum reference pressure of 50 psig. The orifice downstream pressure port is connected to the reference port on the PSI transducer.

The unsteady total pressure at the rotor exit is measured by a high frequency Kulite semiconductor transducer, XCS-062-5D. Reference side of the differential pressure transducer is connected to ambient pressure. The transducer element has a natural frequency of 150 kHz. The sensor is mounted with a screen and is known to have a flat magnitude and phase response up to 20 kHz. The Kulite is flush mounted into a square cut cylindrical probe of diameter 3.5 mm. The probe is located $0.3C_{ax}$ downstream of the rotor exit plane and is oriented to the absolute velocity vector at the tip (25.4° CCW from axial). The probe is positioned such that it is at mid-pitch of the upstream nozzle passage. The probe is mounted in a computer controlled radial traverse system driven by a stepping motor.

Turbine Operation: The air temperature in the test cell experiences a 5-6 ^{o} C rise during a test. Most of this occurs in the first half hour of the turbine run. Additionally, to avoid instrumentation errors due to temperature effects it is necessary to run the turbine at corrected operating speed for some time. A series of tests showed that a time of 45 minutes was sufficient to allow the test cell temperature to sufficiently stabilize and for the instruments to achieve the same temperature. Throughout the run the turbine speed is maintained at the corrected speed for the operating temperature.

For tests involving mass injection, the air supply was turned on after 45 minutes. The injection flow rate was adjusted to the desired value and allowed to stabilize for 5 minutes, before data acquisition was commenced.

Data Acquisition and Processing: All data acquisition is controlled by virtual instruments (VI) setup using LabView. Performance monitoring data is acquired by a National Instruments PCI-6024E, 8 channel DAQ board in a personal computer. A monitor VI records the speed and total pressure, dynamic head, and total temperature at inlet and exit. The speed is measured using the 6000 pulses per revolution signal generated by the shaft encoder. The traverse mechanism and high speed data acquisition for total pressure is controlled by a personal computer with a National Instruments PCI-6110E board. This 12 bit data acquisition module is capable of simultaneously sampling its four channels at a maximum rate of 1.25 Ms/sec. The data acquisition is initiated by a trigger pulse (1 per revolution) and is controlled by a clock pulse (6000 pulses per revolution). Both these digital signals are generated by the BEI optical shaft encoder on the turbine shaft. The data acquisition is thus phase-locked and is conducted at a frequency determined by the temperature corrected rotor speed. Frequency spectra at various locations show three peaks, at the blade passing frequency (BPF) and its harmonics. Additionally, the energy contained in the signal at frequencies above 12 kHz is 20 dB less than that at the 2 BPF and 30 dB less than that at the BPF. Hence, the signal was low-pass filtered at 20 kHz. At each radial location 200 ensembles of the rotor exit absolute total pressure are acquired and averaged. The probe is moved in the radial direction in steps of 1/16 of an inch by a computer driven stepping motor.

The results are presented in the form of a total pressure coefficient, as defined by Equation 1. Radial distributions of the total pressure coefficient are computed as shown in Equation 2 for passage averaged values and Equation 3 for rotor averaged values. The circumferential extent for passage averaging consists of 206 points. A passage is defined for the test blade such that the first point is at the edge of the suction-side of wake due to #20 (C_{pt} = -4.0). The last point in this passage is on the edge of the test blade wake (#21) at the same value of C_{pt}. Other passages are defined relative to the test blade passage. Thus, the passage for #22 starts one data point after the passage for #21 and consists of 206 points.

$$C_{pt}(i,j) = \frac{\overline{P}_{03}(i,j) - P_{01}}{\frac{1}{2}\rho U_m^2} \qquad (1)$$

$$C_{pt,P}(j) = \sum_{i}^{i+206} C_{pt}(i,j) \qquad (2)$$

$$C_{pt,R}(j) = \sum_{i=1}^{6000} C_{pt}(i,j) \qquad (3)$$

MEASUREMENT UNCERTAINTIES

The propagation of uncertainty, calculated as per Kline and McClintock [15], results in an uncertainty of $\delta C_{pt} = \pm 0.024$ (0.58% of the nominal total pressure coefficient). The total pressure sensor used for the rotor exit flow-field measurement has a ±35 Pa absolute measurement uncertainty (± 0.1 % full scale). The dynamic pressure sensor Kulite XCS-062 did not have significant non-linearity error in the narrow range of dynamic pressure encountered in the turbine facility. The mean total pressure at the rotor exit is 94 % of the inlet total pressure that is approximately 6 kPa or 17 % full scale reading of the transducer.

The rotational speed of the rotor in AFTRF was controlled to within ± 1 RPM by an eddy current brake. The stage entry temperature was measured by a K type thermocouple used in a total temperature probe located upstream of the nozzle guide vanes. This temperature measurement had an uncertainty of ± 0.2 K. The tip clearance measurement uncertainty was about ± 25.4 microns. A probe angle of 25.4° to the axial direction was maintained in all total pressure measurements reported in this paper. This angle corresponds to α_3 in the design velocity triangle for the tip region. Angular sensitivity studies were performed in the AFTRF, by rotating the probe in ± 5° increments around the nominal angle setting. It was concluded that within the limits of experimental uncertainty, the probe is insensitive to a flow angle change of ±10°. Some details of this are provided in Appendix (A). Wall interference was a concern for the tip measurements made close to the outer casing. Measurements were not possible in the last 1 % of blade height due to wall proximity effects and probe safety issues.

EXPERIMENTAL RESULTS AND DISCUSSION

Results presented consist of contour plots, circumferential and radial distribution of averaged total pressure coefficient C_{pt}. The term "*Baseline"* refers to tests conducted without tip injection and with the test blade clearance at 1.40%. A total of three baseline cases are presented in this paper. Initially, data was acquired from 0.051h to 0.981h. Subsequently, data was acquired from 0.438h to 0.981h, since it was determined that variations below 0.438h were negligible, within uncertainty limits. The injection mass flow rate is based on the total mass flow that would be injected from all 29 blades. Thus, 0.4% injection means that the mass injected from the test blade is (0.004*turbine mass flow rate/29). It must be noted that the actual mass flow injected through the test blade is 0.014% of the turbine mass flow, for 0.4% injection. The radial distributions of the passage averaged and rotor averaged total pressure coefficients are plotted as continuous curves, rather than points. The curve itself is generated by a three point moving average of the data with the end points unchanged. The passage averaged coefficient is computed for the passage that is bounded on the suction side by the blade number referenced. So, a passage averaged coefficient for the test blade (#21) is the measured total pressure coefficient averaged across the passage that is bounded by the suction-side of #21 and pressure-side of #20.

Baseline Experiments: Figure 3 is a contour plot of the total pressure coefficient measured $0.3C_{ax}$ downstream of the rotor exit plane, designated as Base1. The figure shows C_{pt} details from 5 neighboring passages, with the test blade as marked. The test blade tip clearance is t/h=1.40%. Radial locations corresponding to the hub, the casing, and 50%, 75%, and 85% blade span are shown with solid lines. The tip clearance value t/h, as percent of blade height, of each blade is noted above the casing boundary in the figure. The numbers above the tip clearance indicate the blade number. The direction of rotation is from right to left, as represented by the blade speed vector below the hub boundary. Boundaries are drawn as solid lines around the tip vortex zone to enable easy comparison with results presented later. The dashed lines are used to distinguish the limits of the core flow in the passage. These details are consistently reproduced in all subsequent contour plots.

Baseline Experiments in the Region above 85% Blade Height: This region is dominated by two distinct flow regimes. The tip leakage vortex, seen in the wake region of each blade, is characterized by low total pressure and a near elliptical shape. The shape results from the tip vortex data being projected onto a plane normal to the rotor axis. The leakage vortex of the test blade occupies about 15% of the blade span and extends well into the blade passage. The vortex has a well defined core and strong gradients in both radial and circumferential directions. The total pressure at the core is approximately 0.2 q_m. The minimum test blade total pressure, measured in the core of the tip vortex, is lower than that of the neighboring blades shown because of the specific tip clearance value of this blade. In general, the size of the leakage vortices and the minimum total pressure relate well with the blade clearance. The entrainment of low momentum fluid by the leakage flow and diffusion beyond the rotor exit plane has caused the blade wake to be completely overshadowed by the leakage flow. In each of the passages the lowest total pressure is measured in the core of the tip vortex.

The second distinct flow region in the last 15 % blade height is the intermediate total pressure zone between the two adjacent tip vortices. This zone (C_{pt}=-3.85, green) is bounded by the outer casing that is in relative motion with respect to rotating passage, the core flow in the middle of the passage and the two subsequent tip vortices. The secondary flow pattern near the outer casing is more distorted in comparison to its counterpart near the hub surface because of the leakage flow. Velocity measurements by McCarter et al. [16] show higher axial and reduced tangential velocities in this region. This is consistent with under-turning of the passage flow due to blockage and secondary flow effects. Such under-turning would be the greatest in the passage containing the test blade leakage vortex.

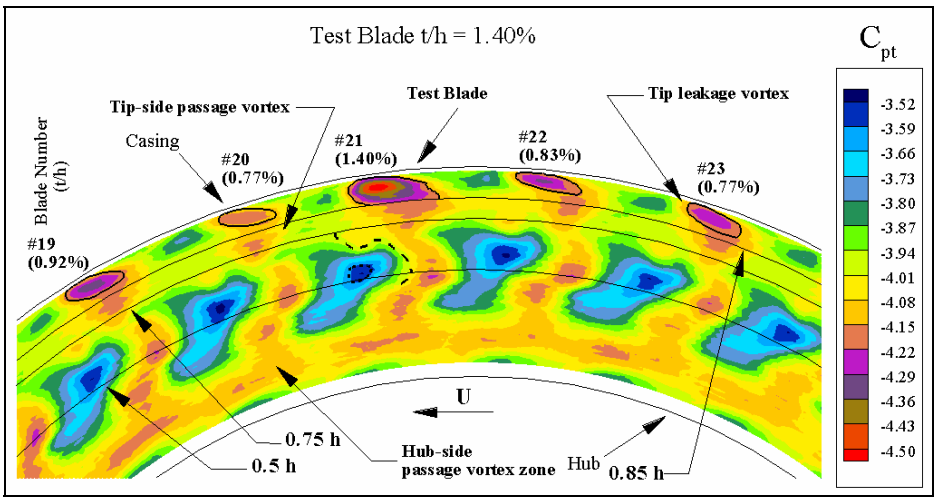

Figure 3 Base1: t/h = 1.40%, M_{inj} = 0

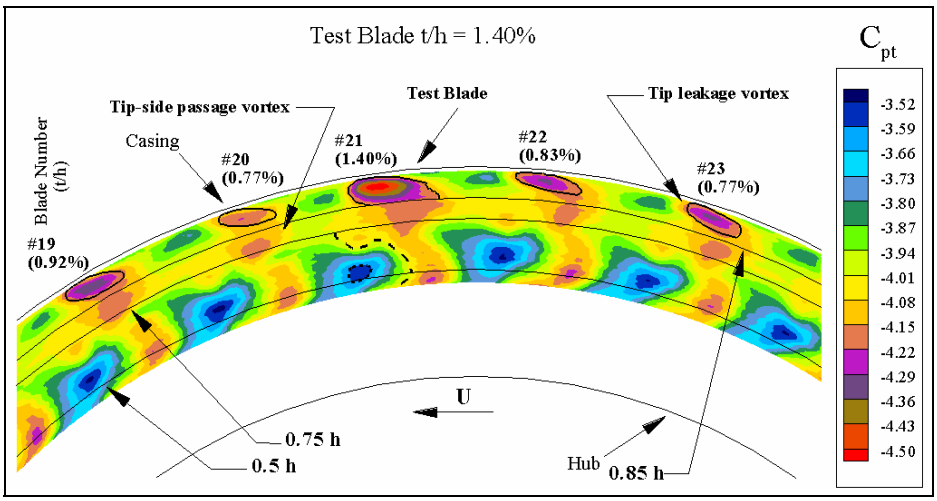

Figure 4 Base3: t/h = 1.40%, M_{inj} = 0

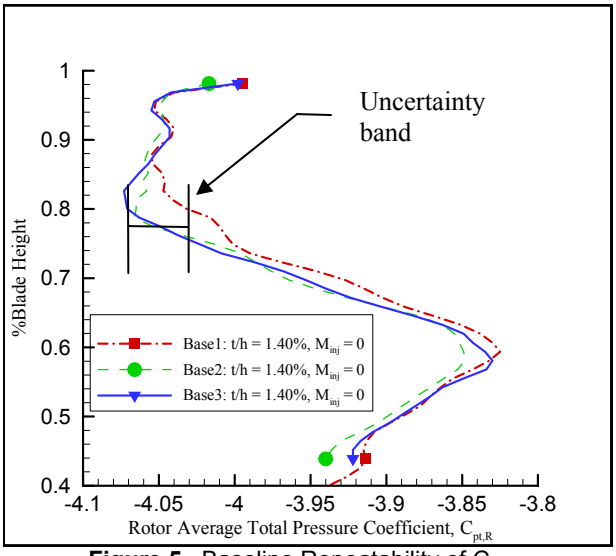

Figure 5 Baseline Repeatability of $C_{pt,R}$

Baseline Experiments in the Region within 75% - 85% Blade Height: The main flow feature present in this region is the tip-side passage vortex, as marked in Fig. 3. The identity of this structure is also confirmed by results in McCarter et al. [16]. It exists just below the tip leakage vortex and has a minimum total pressure greater than that of the leakage flow. The interaction of the passage vortex with the leakage vortex is greatest for the test blade, as seen by the poor definition of the passage vortex in the wake. Another interesting characteristic of this region is a band of lower total pressure that runs across the passage, culminating in the passage vortex. This suggests that the secondary flow effect is greatest in this region, with the flow probably being over-turned as it migrates towards the suction side of the passage.

Baseline Experiments in the Passage Core and Hub Side Passage Vortex: The passage core occupies about 50% of the passage height. It has a well defined core of high total pressure around 50% blade height. Just below 75% span, close to blade suction-side, a dip in the passage core is observed. This is possibly due to a vortical structure. The extent of the dip suggests that this structure is formed early in the blade passage and is convected downstream. Below 50% span the passage core is strongly affected by the hub-side passage vortex, which rotates in the same direction as the leakage vortex. Although the hub-side passage vortex is not as clearly discernible as the tip-side passage vortex, its effect on the passage core is clear. A better definition of the hub-side passage vortex is clearly observed in the past, phase-locked LDA measurements obtained by Ristic et al. [17] in the same facility. It must be noted that the nominal absolute flow angle at the hub is 35°, which is a 10° incidence on the probe. Additionally, the passage flow tends to be over-turned closer to the hub, due to the hub-side passage vortex. In the passage containing the test blade, the passage core is shifted radially downwards, probably by migration of fluid towards the hub due to the blockage of the tip leakage vortex. The core in the passage formed by #21 & #22 is at a higher radius, suggesting a strong radial flow towards the tip due to the enlarged clearance of the test blade.

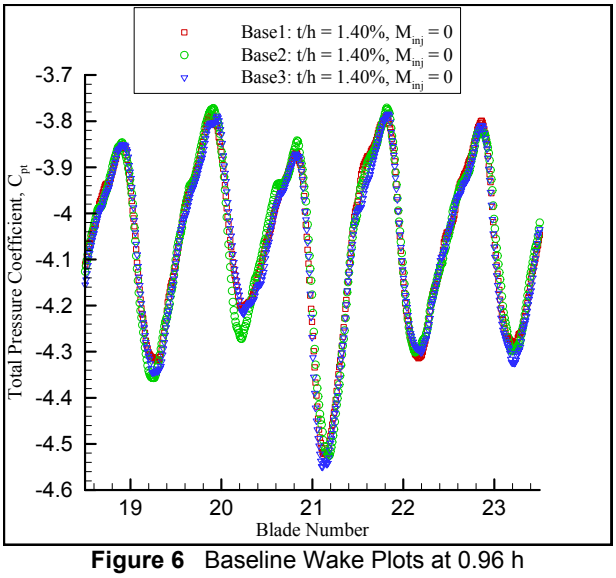

Figure 6 Baseline Wake Plots at 0.96 h

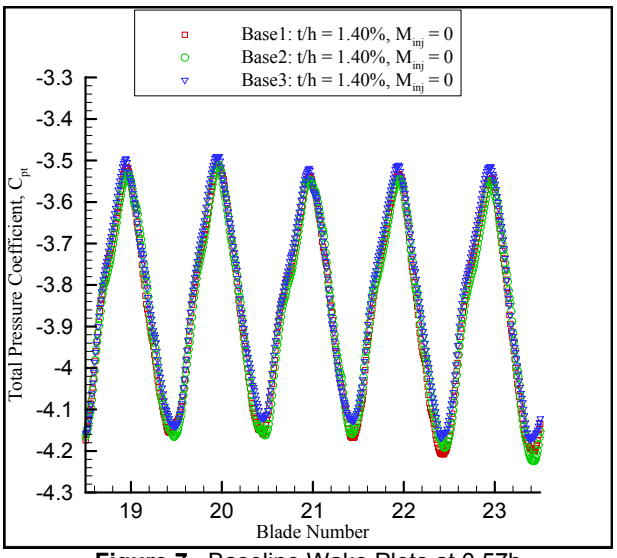

Figure 7 Baseline Wake Plots at 0.57h

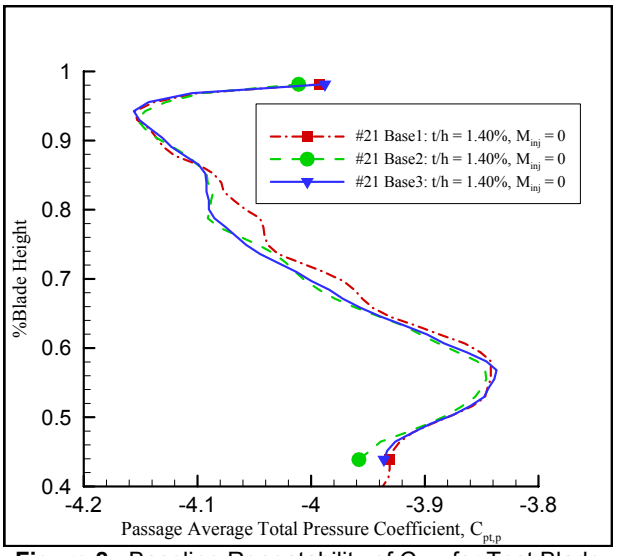

Figure 8 Baseline Repeatability of $C_{pt,P}$ for Test Blade

Baseline Repeatability: Data from the three baseline tests are presented for repeatability purposes. Figure 4 is a contour plot of Base3 and compares well with Fig. 3 for Base1. Circumferentially averaged total pressure coefficients along all 29 passages in the rotor are shown in Fig. 5. All three baseline cases are presented. In the tip vortex dominated zone and core of the passages the repeatability is sufficiently maintained for three baseline experiments performed at different dates. These repeatability experiments were run 2 months apart from each other. While general repeatability is good, the region between 70% and 80% blade height shows higher uncertainty for Base1. Figure 5 shows reasonably good repeatability within a 95% confidence level for the measurements.

Figures 6 and 7 show phase-averaged total pressure profiles obtained at r/h=0.96 and 0.57 for the passages defined by the blades (#'s 19, 20, 21, 22, 23). The circumferential distributions obtained at a fixed radial position are termed as "wake plots" throughout the manuscript. The wake plots at r/h=0.96 and 0.57 further attest to the repeatability of the experiments.

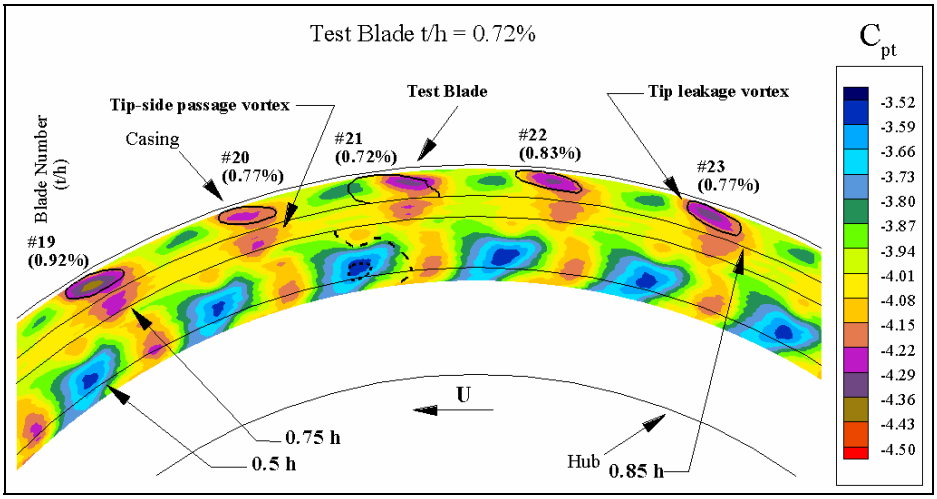

Figure 9 t/h = 0.72%, M_{inj} = 0

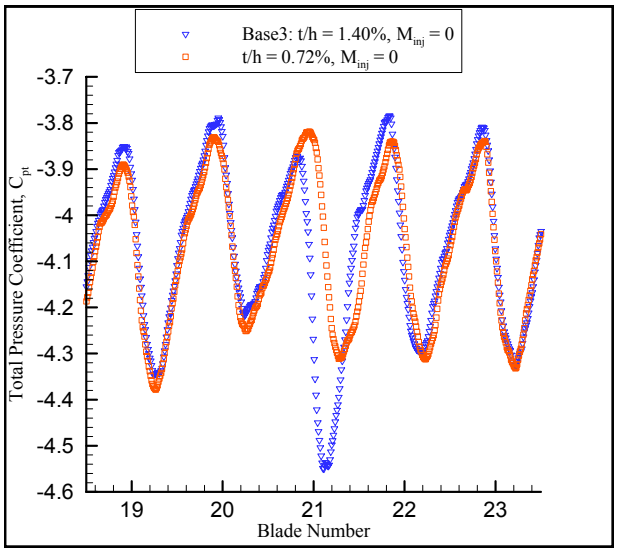

Figure 10 Influence of Tip Gap Height on C_{pt} at 0.96h

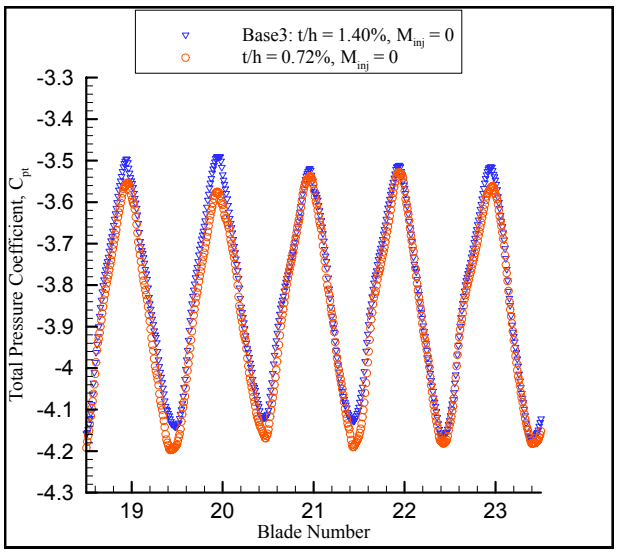

Figure 11 Influence of Tip Gap Height on C_{pt} at 0.57 h

These locations correspond to the locations of leakage vortex dominated zone and core flow where there is minimal tip vortex influence. Overall, the repeatability is very good at both radial locations. The influence of the test blade with a relatively large tip clearance of 1.40% is visible in Fig. 6 as the minimum total pressure dip induced by the tip vortex. However, when the same distribution at a lower radius (r/h=0.57) is examined, the tip vortex influence diminishes. Excellent repeatability of the total pressure data is presented in Fig. 7 where r/h=0.57. Circumferentially averaged total pressure coefficients for the passage defined by #20 and #21 (test blade) are shown in Fig. 8. The radial distribution of $C_{pt,P}$ shown in Fig. 8 is very similar to the results from all 29 passages (rotor averaged) presented in Fig. 5 except that the tip region results are influenced by the large tip clearance of #21 with t/h=1.40%. The effect of the increased clearance of the test blade is smoothed out in the rotor averaged coefficient, and hence the peak in the passage averaged coefficient distribution for r/h>0.85 may be interpreted as a total pressure deficit zone.

Effect Of Tip Gap Height With No Injection: Figure 9 shows a contour plot of C_{pt} when the test blade tip clearance is reduced to t/h=0.72% from t/h=1.40%. The effect of reducing the tip clearance is evident in the distribution and level of measured total pressure at stage exit. The solid lines marked around the tip vortex zones are from the baseline case and used for comparison purposes. The tip leakage vortex, due to the test blade, is much smaller in size and closer to the suction-side of the passage when t/h=0.72%. The total pressure in the vortex is higher than that of the baseline by about 0.2 q_m. The passage flow above 85% span should experience less under-turning and hence register as a higher absolute total pressure, in comparison to the baseline. The passage vortex (casing side) of the test blade is better defined. The passage core itself has rotated in a counterclockwise direction due to the reduced blockage of the leakage flow. The tip leakage vortices from the neighboring blades maintain their location.

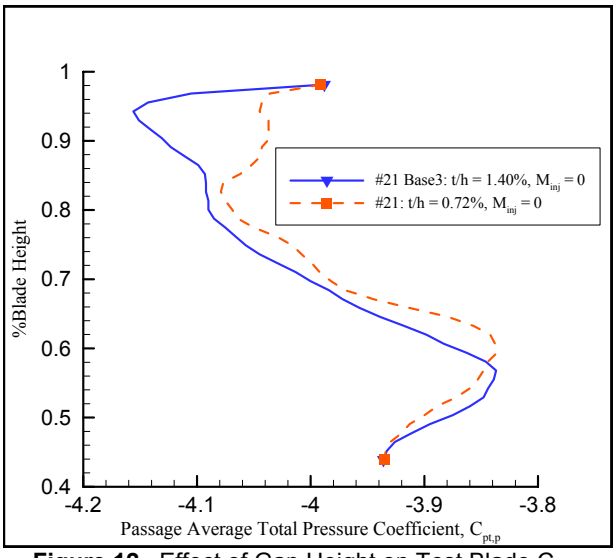

Figure 12 Effect of Gap Height on Test Blade $C_{pt,P}$

The wake plot presented in Fig. 10 clearly shows the movement of the tip vortex from the test blade towards the suction-side of the blade. This figure is presented from data sampled at r/h=0.96 where the tip vortex is influential. The blue triangles indicate a significant total pressure defect in the tip vortex when the clearance is large, at t/h=1.4%. The total pressure deficit is reduced (orange squares) and compares well with that of the neighboring blades. The reduced blockage due to the tip leakage flow also changes the behavior of the passage flow near the casing. Figure 11 evaluated at r/h=0.57 shows a slight drop in the total pressure at the mid-span. This is due to the aforementioned rotation in the passage flow due to a reduction in the influence of the leakage flow on the passage flow. Tip vortex impact at this lower radial position is not measurable in the passage of the test blade.

The radial distribution of the passage averaged pressure coefficient, Fig. 12, shows that, in addition to the significant increase in the total pressure, there is a definite shift in the profile towards the blade tip. This confirms that the lower total pressure seen in the wake plots is due to a change in the passage flow structure. The loss peak due to the tip-side passage vortex is better defined than in the baseline because the tip vortex/passage vortex interaction is reduced when the tip gap is reduced to t/h=0.72% .

Effect Of Tip Coolant Injection: This section presents results for injection mass flow rates of M_{inj}=0.41%, 0.52%, 0.63%, and 0.72% of core flow, at test blade t/h=1.40%. Injection is initiated only at the test blade tip. Injection at M_{inj}=0.41% of core flow significantly reduces the tip leakage flow as shown in Fig. 13. The minimum total pressure in the wake increases by about 0.2 q_m. This effect is similar in magnitude to that obtained with reduced tip clearance of t/h=0.72% but no injection. However, the flow structure is less like a vortex with a smaller pitch-wise footprint. When the injection rate is increased to 0.52%, Fig. 14, the behavior is essentially the same. Note that in both cases the interaction between the leakage vortex and the tip-side passage vortex is still strong enough that the passage vortices of the test blade are not well defined. Further increasing the injection rate to 0.63%, Fig. 15, shows a few interesting changes in the flow structure. The tip leakage from the test blade is not only reduced, but also lifted more towards the casing. The tip-side passage vortex of the test blade is starting to show better definition, indicating lesser interaction between the two flow structures. The behavior of the flow is tending towards that of reduced clearance. Injection also affects the tip leakage vortex due to #22. The tip vortex is seen to move towards the suction side of #22. This effect is more noticeable in the 0.72% injection case, Fig. 16, where the tip leakage flow from #23 is also affected, although to a lesser extent. The leakage vortex of #22 is greatly reduced in size and also diffused. The most dramatic change here is the position of the leakage vortex of #22 in relation to the tip passage vortex. In the baseline it was shown to be inside the tip passage vortex, while injection at 0.72% has actually moved it to the outside, probably due to jet penetration.

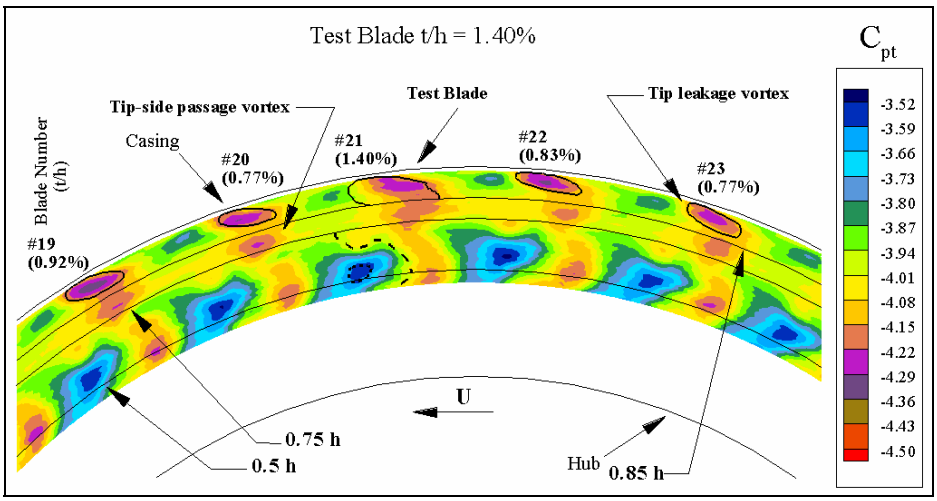

Figure 13 t/h = 1.40%, M_{inj} = 0.41%

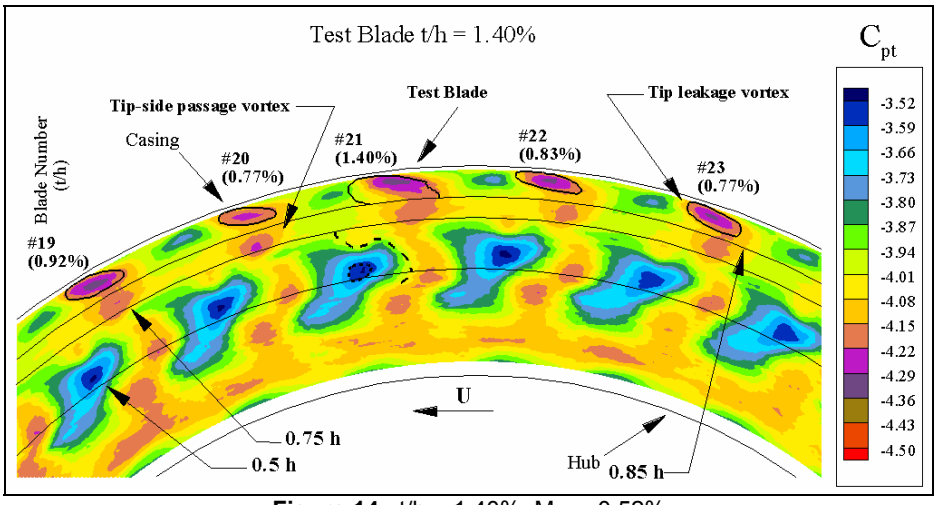

Figure 14 t/h = 1.40%, M_{inj} = 0.52%

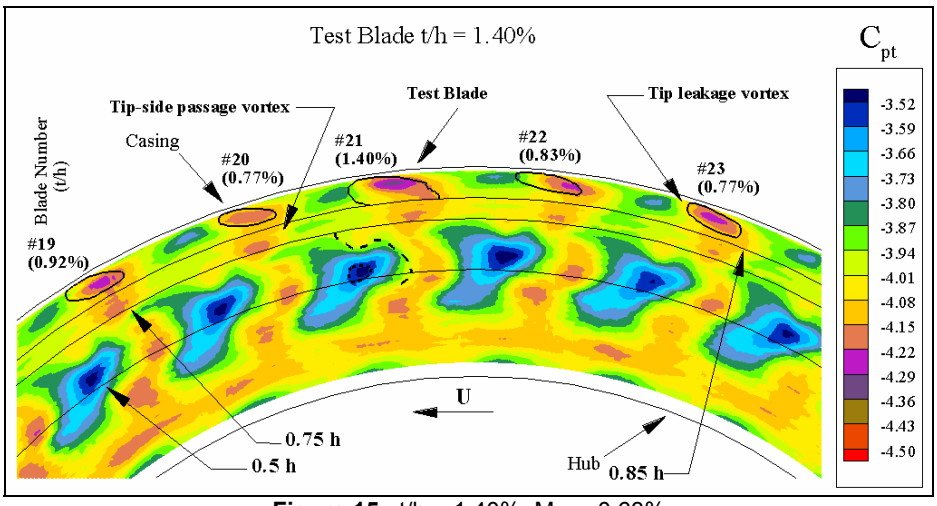

Figure 15 t/h = 1.40%, M_{inj} = 0.63%

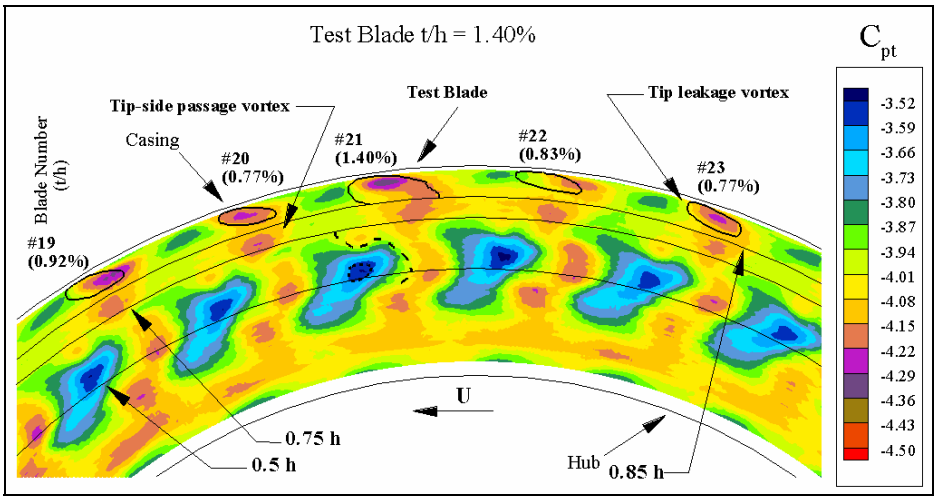

Figure 16 t/h = 1.40%, M_{inj} = 0.72%

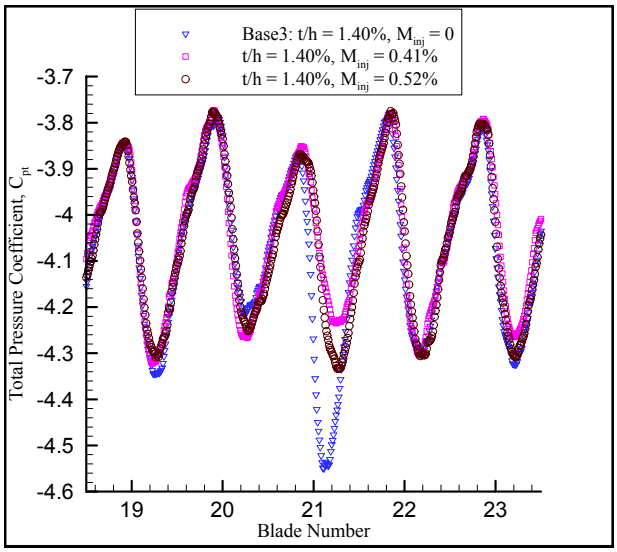

Figure 17 Influence of Injection (M_{inj} = 0.41% & 0.52%) on C_{pt} at 0.96h

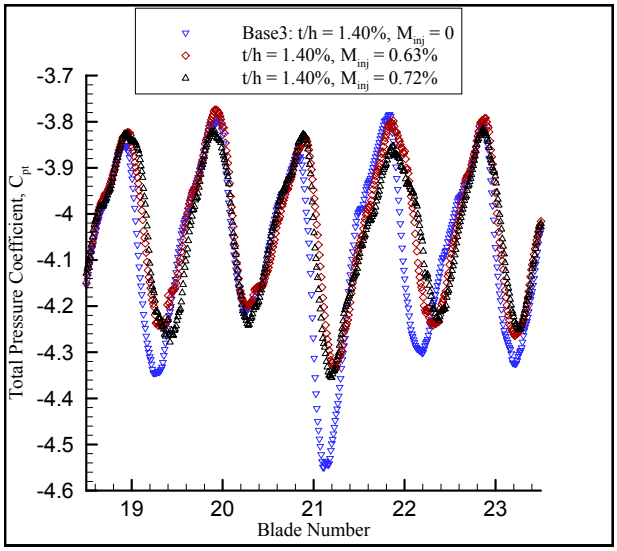

Figure 18 Influence of Injection (M_{inj} = 0.63% & 0.72%) on C_{pt} at 0.96 h

In all cases, the passage core flow is not affected much, as seen by the curves representing the baseline. The passage flow above 85% shows minimal indication of reduced under-turning, as in the case with reduced tip clearance. This suggests that most of the under-turning results from the leakage flow in the forward part of the blade and the influence of the passage vortex, rather than the leakage vortex itself.

The wake plots comparing the baseline and the tip injection are shown in Figures 17 and 18. Figure 17 compares Base3 with tip injection rates of M_{inj}=0.41% and 0.52% at r/h=0.96. The figure shows that in both cases of tip injection the total pressure defect is reduced and the C_{pt} minimum moves slightly against the direction of rotation. However, as opposed to the reduced tip clearance case, the shift is minimal. Tip injection rate of 0.41% shows the greatest reduction in total pressure defect. The wake profiles of the neighboring blades remain essentially the same. A further increase in tip injection rate to M_{inj}=0.52% starts reducing the benefits of tip injection as shown in Fig. 17. Figure 18 compares Base3 (no injection) to tip injection rates of 0.63% and 0.72% at r/h=0.96. While the total pressure defect is somewhat reduced, the effectiveness in filling the defect in the total pressure profile diminishes when compared to the case with M_{inj}=0.41%.

Figure 19 compares all injection cases with a no-injection case (Base3) at t/h=1.4% and r/h=0.57. The circumferential distributions of C_{pt} show that there isn't much deviation from the baseline at this radial position where the tip vortex or tip injection influence is minimal. Tip injection in a wide range of M_{inj} from 0.41% to 0.72% does not influence the passage flow near the core of the passage below r/h=0.57.

A final comparison is made of the radial distribution of the passage averaged total pressure coefficient in Fig. 20. All injection rates show similar patterns with the major difference being that at 0.41%, the total pressure above 90% span does not show a distinct peak. The profile is reasonably flat from 75% span up to 90% span, at M_{inj} = 0.63%. A distinctive peak above 90% span is present. This case shows the greatest total pressure recovery in comparison to the baseline, especially in the region of the tip-side passage vortex.

Comparison of Blade #7 & Blade #21: This section compares the passage averaged pressure coefficient of #7 and #21(test blade). Blade #7 is almost diametrically opposite to blade #21 and has a tip clearance of t/h=0.71%. Figure 21 compares the radial distribution of $C_{pt,P}$ for the baseline and the reduced test blade tip clearance cases. It is seen that after reducing the test blade (#21) clearance to 0.72% the radial distribution matches that of #7. Blade #6 and #8 have gap height of t/h = 0.73% and t/h = 0.71%, respectively. Blade #20 and #22 have gap height of t/h = 0.77% and t/h = 0.83%, respectively. Thus, it appears that the gap height of neighboring blades has little influence on the passage averaged total pressure, as long as the variation in gap heights is within 15%.

In the studies reported in this two part paper only one blade was modified in order to isolate the effect of injection. Indeed, changing the gap height of, and initiating coolant injection from a single blade does affect the neighboring passages. This effect is however localized close to the test blade. Also, the effect of the neighboring blades on the leakage over the test blade is expected to be small, in comparison to the effect of the large disturbance caused by the test blade. This ensures that there is not a substantial change in the stage behavior, allowing for a fair comparison of the effect of injection with that of changing gap height.

Investigation of the effect of changing gap height and coolant injection from all five modified blades is in progress. It is expected that this will allow measurable changes in the work output. Additionally, the effect of injection at the higher mass flow rates is expected to be more pronounced.

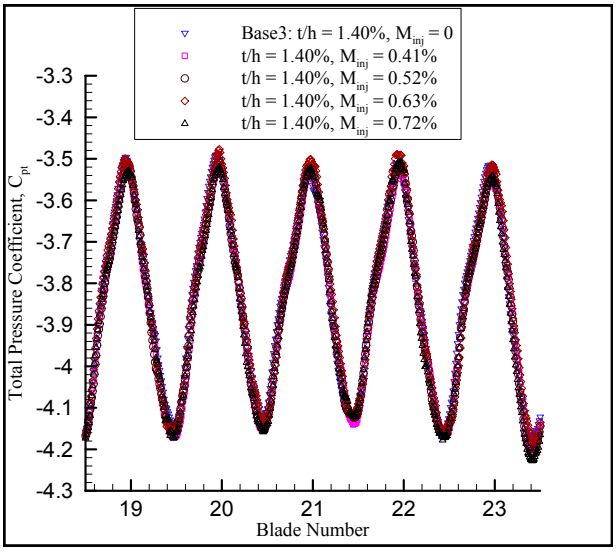

Figure 19 Influence of Injection on C_{pt} at 0.57h

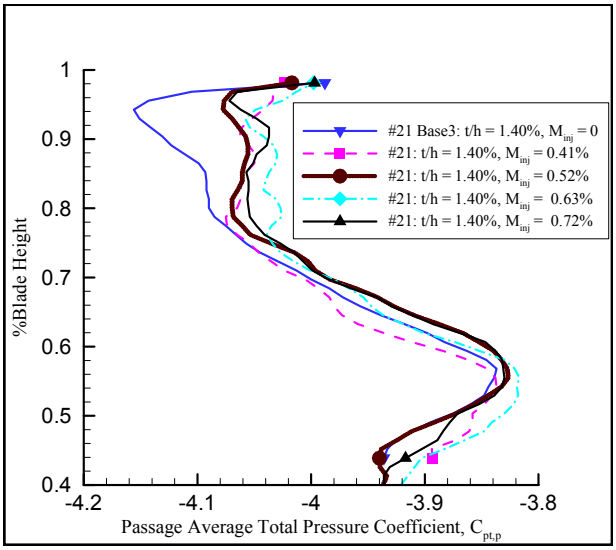

Figure 20 Effect of Injection on Test Blade $C_{pt,P}$

CONCLUSIONS

An experimental investigation of a turbine tip desensitization method based on tip coolant injection was conducted in a large-scale rotating turbine rig. One of twenty-nine rotor blades was modified to, have a tip trench with discrete injection holes directed towards the pressure side. The current paper focuses on the influence of tip injection mass flow rate using all four injection locations named H1, H2, H3

and H4, simultaneously. All four locations are fed from the same plenum chamber located at the root of the test blade.

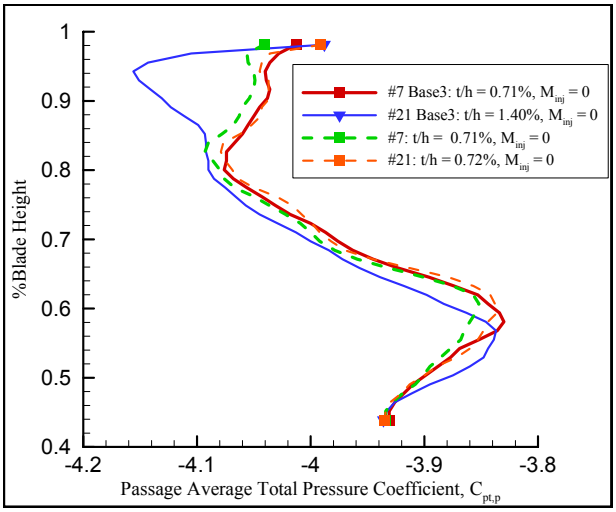

Figure 21 Comparison of $C_{pt,P}$ for #7 and #21.

A complete mapping of the rotor exit total pressure field for all 29 passages is possible. The total pressure probe attached to the outer casing of the turbine stage is traversed in radial direction. Distinct flow structures such as tip vortices, passage vortices, blade wake and core flow can be detected by employing a phase-locked ensemble averaging technique.

Time accurate absolute total pressure was measured $0.3C_{ax}$ downstream of the rotor exit plane using a fast response dynamic pressure sensor in a phase-locked manner. The test cases presented include results for tip gap heights of t/h=1.40% and 0.72% of the blade height, and coolant injection rates M_{inj}=0.41%, 0.52%, 0.63%, and 0.72% of core mass flow rate. At a gap height of t/h=1.40% the leakage vortex is relatively large, occupying about 15% blade span. The tip vortex for this case presents a significant blockage to the passage flow. The flow under-turning due to this is clearly seen in the measurements, as is the effect of inward flow towards the hub.

Reduction of tip clearance effectively reduced the blockage presented by the tip clearance flow to the passage flow. The total pressure drop measured in the leakage vortex is reduced by about 20% q_m. The size of the leakage vortex is greatly reduced, by almost 50%, at the smaller gap height. The reduced interaction between the leakage vortex and the passage vortex is evident by the better definition of the passage vortex. A reduction in tip gap height also causes the leakage vortex to move towards the blade suction-side.

Coolant injection from the tip trench is successful in filling in the total pressure defect originally resulting from the leakage vortex without injection. Injection mass flow rates of 0.41%, 0.52%, 0.63%, and 0.72% were investigated.

At all injection rates, the reduction in total pressure deficit is very similar to that when the gap height t/h=1.40% is reduced by half to 0.72%. This result shows that tip injection jets can be effective in creating beneficial effects previously observed only from small clearances.

Injection at M_{inj}=0.41% core flow was the most effective in reducing the total pressure loss in the leakage flow of the test blade. This was observed at a radius near the core of the tip vortex. However, it appears that 0.63% injection is the most effective from a global point of view, as shown by the passage averaged pressure coefficient obtained in the last 25 % of the blade height. At injection rates of 0.63% and 0.72% the momentum of the jets was high enough to affect the tip leakage flow of adjacent blades.

The tip leakage vortex moves closer to the tip in radially outward direction, especially at the higher injection rates. The cross section of the new tip leakage vortex, with injection, is smaller and some of the total pressure defect is eliminated by the injection process. The upper passage vortex is better defined when the tip leakage vortex cross section is smaller and located nearer the casing.

The relatively high radial position of the leakage vortex resulting from M_{inj} values 0.63% and 0.72% implies that the interaction with the passage vortex is less pronounced. Thus, tip injection is capable of reducing losses, especially those due to leakage flow/passage vortex/blade wake interaction.

At the two highest injection rates the leakage vortices of adjacent blades (to the right of the test blade) are affected by the injection. The high momentum associated with these jets moves the tip vortices in adjacent channels against the direction of rotation. This might be due to the alteration of the near casing flow between the pressure side corner of the test blade and the adjacent blade. Since the tip jets are faced towards the pressure side corner of the test blade, especially at high blowing rates, the static pressure distribution near the outer casing in the adjacent passage is expected to be altered.

ACKNOWLEDGMENTS:

The research effort was initiated during our early discussions with Drs. B. Glezer and R. Bunker. The authors are thankful to Drs. L. Golan and R. Wenglarz of SCIES/HEET for their initial support. The mechanical design, manufacturing and assembly of the tip cooling system were possible because of the continuous involvement of Dr. D. Dey, G. Sayers and H. Houtz in Penn State. The authors are also indebted to late Prof. Lakshminarayana for his constructive criticism and suggestions over the years the AFTRF was developed into a fully operational turbine research facility.

NOMENCLATURE

C_{ax}	Rotor tip axial chord length = 0.08514 m
C_{pt}	Pressure coefficient $C_{pt}(i,j) = \frac{\overline{P}_{03}(i,j) - P_{01}}{0.5\rho U_m^2}$
M_{inj}	Coolant to free stream mass flow rate ratio
U_m	Mean wheel speed at rotor mid-span, m/sec
h	Rotor blade height = 0.123 m
i	Circumferential index
j	Radial index
p_{o1}, P_{o1}	Stage inlet total pressure, Pa
p_{o3}, P_{o3}	Stage exit total pressure, Pa
r/h	Non-dimensional radial position measured from hub
q_m	Mean kinetic energy based on U_m, Pa
t	Gap height between blade tip and outer casing, m
α_3	Rotor exit abs. velocity vector angle at tip, degrees
ϕ	Diameter of injection hole, mm
ρ	Density, kg/m^3
#	Blade number

REFERENCES

1. Bindon, J. P., 1989, "The Measurement and Formation of Tip Clearance Loss," ASME J. of Turbomachinery, **111**, pp. 257-263, Paper No. 88-GT-203.
2. Booth, T. C., Dodge, P.R., Hepworth, H.K.., 1982, "Rotor-Tip Leakage: Part 1- Basic Methodology," ASME J. of Eng. For Power, **104**, pp. 154-161, Paper No. 81-GT-72.
3. Bindon, J. P., 1987, "Pressure Distributions in the Tip Clearance Region of an Unshrouded Axial Turbine as Affecting the Problem of Tip Burn-out," ASME Paper No. 87-GT-230.
4. Bunker, R. S., "A Review of Turbine Blade Tip Heat Transfer," Presented at International Symposium "Turbine 2000" on Heat Transfer in Gas Turbine Systems, August 13-18, Cesme, Turkey.
5. Yang, H., Acharya, S., Ekkad, S., 2002, "Flow and Heat Transfer Predictions for a Flat-Tip Turbine Blade," ASME Paper No. GT-2002-30190.
6. Dey, D., 2001, "Aerodynamic Tip Desensitization in Axial Flow Turbines," Ph.D. Thesis, 2001d, The Pennsylvania State University.
7. Dey, D. and Camci, C., 2001, "Aerodynamic Tip De-sensitization of an Axial Turbine Rotor Using Tip Platform Extensions," ASME paper 2001-GT-484.
8. Camci, C., Dey, D. and Kavurmacioglu, 2003,"Tip Leakage Flows Near Partial Squealer Rims in an Axial Flow Turbine Stage," ASME paper 2003-GT-38979.
9. Dey, D., Camci, C., 2000, "Development of Tip Clearance Flow Downstream of a Rotor Blade With Coolant Injection From a Tip Trench," In Proceedings of the 8th ISROMAC Conference, Honolulu, Hawaii pp. 572-579.
10. Tallman, J., Lakshminarayana, B. L., 2001, "Methods for Desensitizing Tip Clearance Effects in Turbines," ASME Paper No. 2001-GT-0486.
11. Ameri, A.A., 2001, "Heat Transfer and Flow on the Blade Tip of a Gas Turbine Equipped with a Mean Camberline Strip," ASME J. of Turbomachinery, **123**, pp.704-708, Paper No. 2001-GT-0156.
12. Bunker, R.S., Bailey, J.C., 2000, "Blade Tip Heat Transfer and Flow with Chord-wise Sealing Strips," International Symposium on Transport Phenomena and Dynamics of Rotating Machinery (ISROMAC), Honolulu, Hawaii, pp.548-553.
13. Chen, G., Dawes, W. N., Hodson. H. P., 1993, "A Numerical Investigation of Turbine Tip Gap Flow," AIAA 93-2253, AIAA/SAE/ASME/ASEE, 29th Joint Propulsion Conference & Exhibit, June 28-30, 1993, Monterey, CA.
14. Lakshminarayana, B., Camci, C., Halliwell, I., Zaccaria, M., 1996, "Design and Development of a Turbine Research Facility to Study Rotor-Stator Interaction Effects," International Journal of Turbo and Jet Engines, **13**, pp.155-172.
15. Kline, S. J., McClintock, F. A., 1953, "Describing Uncertainties in Single-Sample Experiments," Mechanical Engineering, **75**, pp.3-8.
16. McCarter, A., Xiao, X., Lakshminarayana, B., 2000, "Tip Clearance Effects in a Turbine Rotor: Part 2-Velocity Field and Flow Physics," ASME Paper No. 2000-GT-477.
17. Ristic, D., Lakshminarayana, B., Chu, S., 1998, "Three-Dimensional Flow Field Downstream of an Axial Flow Turbine Rotor," AIAA paper 98-3572, presented at the 34th AIAA/ASME/SAE/ASEE Joint Propulsion Conference and Exhibit, Cleveland, Ohio.

APPENDIX A: Measurement sensitivity to exit flow angle

Measurement sensitivity to exit flow angle was measured in the AFTRF by rotating the probe in increments of 5°, on either side of $\alpha_3 = 25.4°$. This was done at two radial locations, 0.93h (near tip region) and 0.49h (mid span). Counterclockwise (CCW) rotation of the probe is positive and makes the probe more tangential with every increment. The rotor averaged, and passage averaged C_{pt} for #21, are shown in Fig. A-1. The absolute velocity vector at mid span is at an angle of 29.19° from axial, corresponding to an incidence angle of 3.79°. The mean value of $C_{pt,P}$ in a ±15° range is -3.916 and all values in this range lie within the uncertainty band of $\delta C_{pt} = \pm 0.024$. Furthermore, #21 behaves almost identically as the rest of the rotor. At 0.93h however, the difference between the rotor averaged and passage averaged values is considerable. Values from -25° to 10° are within uncertainty limits of the mean value ($C_{pt,P} = -4.22$), computed for the range ±15°. The value at 15° is just outside the uncertainty band. McCarter, et al. [16] measured lower relative tangential velocity in the region dominated by the leakage vortex. This means that the leakage vortex approaches the probe at a negative incidence. Thus, from measurements in the range of -25° to 0° it is possible to conclude that error in the measurement of total pressure associated with the tip leakage vortex of the test blade is within uncertainty bounds.

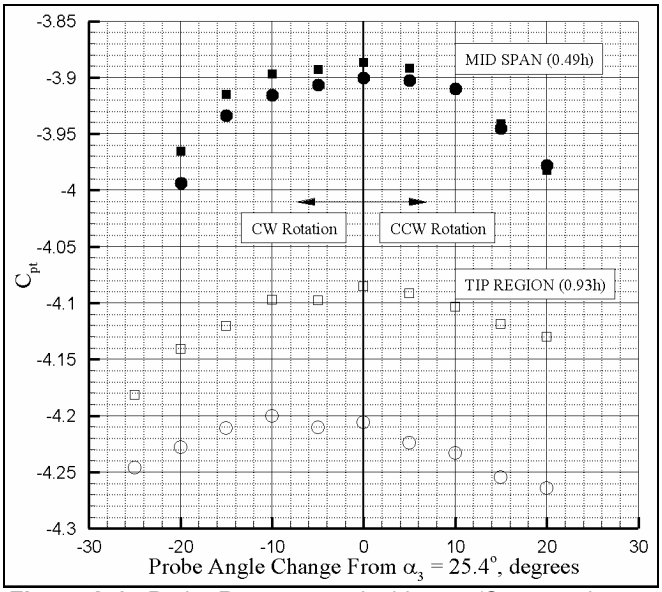

Figure A-1 Probe Response to Incidence. (Squares denote rotor averaged C_{pt} and circles denote passage averaged C_{pt}.)